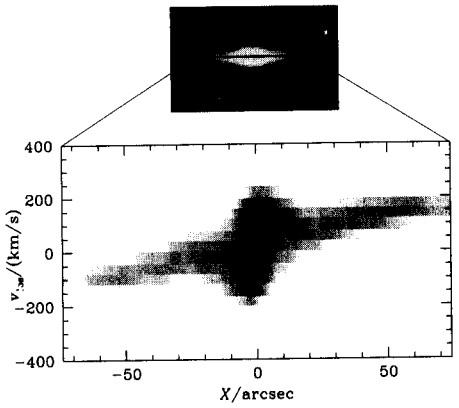

Figure 11.15 Stellar position–velocity diagram for the major axis of the edge-on S0 galaxy NGC 7332 (as shown in the top panel). The grayscale indicates the density of stars as a function of both line-of-sight velocity and position along the major axis. The kinematics were derived using the UGD algorithm. [DSS image from the Palomar/National Geographic Society Sky Survey, reproduced by permission; the kinematic data were obtained by M. Merrifield and K. Kuijken]

11.3 The stellar kinematics of disk galaxies

On account of the multiplicity of components that make up disk galaxies, the interpretation of the kinematics of these systems is more complicated than that of ellipticals. Figure 11.15 shows the PV diagram for the major axis of an edge-on disk galaxy. Close to the center of this galaxy, the light is dominated by the bulge component, so the PV diagram shows a high density of stars which are spread by their random motions to both positive and negative velocities (where, once again, we are measuring velocities relative to the systemic velocity of the galaxy). At large radii, the signature of the rotationally-supported disk is readily apparent in the high density of stars traveling at close to the local circular speed. However, as we shall see below, there are significant random stellar motions even in the disk. Further, the line-of-sight component of the circular speed varies along the line of sight through this edge-on galaxy. We therefore find that the populated region of the PV diagram for this system has a finite spread in line-of-sight velocities even where the disk component dominates. At intermediate radii, there are contributions to the PV diagram from both the disk and the bulge, and the LOSVDs become quite complex. Indeed, analyses of the full LOSVDs of disk galaxies at such radii have shown that these distributions are highly non-Gaussian – the observed skewed distributions have been successfully decomposed into a rapidly-rotating disk component plus a slowly-rotating bulge component [Kuijken & Merrifield (1993), Scorza & Bender (1995); see Problem 11.5].

The complex kinematic structure of a disk galaxy becomes more apparent when one obtains a complete stellar-kinematic data cube by mapping the LOSVD all across its face (see §11.1.3). Figure 11.16 shows kinematic parameters derived from such a data cube in the central region of the edge-on disk galaxy M104 (the Sombrero Galaxy). Along the major axis, the signature of the disk shows up clearly in both the mean streaming motion and the skewness parameter, h_3. The difference in sign between $\overline{v}_{\rm los}$ and h_3

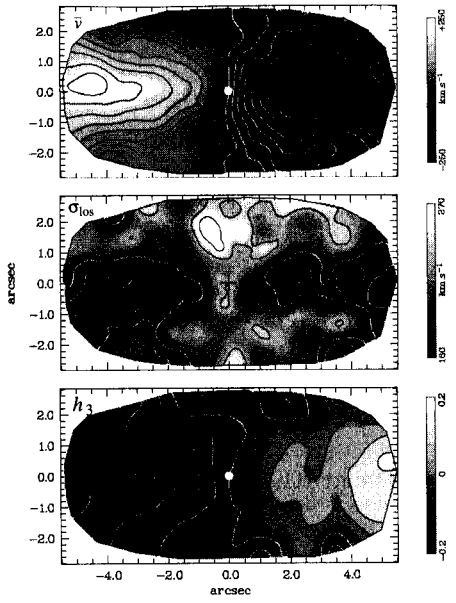

Figure 11.16 A kinematic map of the central region of M104 (the Sombrero Galaxy), showing the variation in mean velocity, line-of-sight dispersion, and skewness with position. The major axis of the system runs horizontally across each panel, with the photometric center of the galaxy indicated. The range of the grayscale is shown to the right of each panel. [After Emsellem et al. (1996) courtesy of E. Emsellem]

reflects the concentration of stars at close to the circular speed, with a tail of stars stretching back towards the galaxy's systemic velocity (see Figure 11.5, and Problem 11.6). Since the disk component is dominated by streaming motions, it depresses the values of $\sigma_{\rm los}$ close to the major axis. Away from the plane of the disk, the light comes mostly from the bulge component, in which random motions dominate, and so $\sigma_{\rm los}$ is larger. The enhancement in $\sigma_{\rm los}$ at very small radii in this galaxy has been successfully modeled by Emsellem, Monnet & Bacon (1994) as arising from a central black hole (see §11.2.2) with a mass of $\sim 10^9\,\mathcal{M}_\odot$.

11.3.1 Bulge kinematics

The kinematics of a galactic bulge are somewhat harder to determine than are the kinematics of an elliptical galaxy: light from the surrounding disk contaminates the observable properties of the bulge, and obscuration due to dust frequently further complicates the analysis. On the positive side, however, the presence of a disk with measurable inclination defines a direction which might reasonably be expected to define one of the principal axes of the bulge – a piece of information that is generally difficult to obtain in the case of elliptical galaxies.

Observations of the bulge of a disk galaxy that lies reasonably close to face-on allow us to measure its central velocity dispersion with little contamination from the disk. Combining such kinematic measurements with the bulge's gross photometric properties suggests that these systems respect

the same fundamental plane as elliptical galaxies (see §4.3.4), and therefore satisfy the standard $D_n - \sigma$ relation of equation (4.43) (Dressler 1987). This similarity between the properties of bulges and ellipticals presumably reflects some common aspect of their formation and evolution, but since we do not yet have a clear understanding of the nature of the fundamental plane, the significance of this discovery is still unclear.

As we have discussed above, the contribution to the total luminosity from the disk increases as we look to larger distances from the center of the galaxy. On these larger scales it therefore becomes difficult to isolate the bulge kinematics in the PV diagram. One solution to this problem is to observe early-type disk galaxies in which the bulge is so dominant that disk contamination is small, but the large bulges which can be observed by this approach may not be representative. Alternatively, observations of the bulges of edge-on galaxies, such as that shown in Figure 11.16, can be used: the surface brightness of the disk drops rapidly with distance from the galaxy's plane (§4.4), so we see fairly pure bulge kinematics in regions away from the major axis of an edge-on system.

Kinematic maps derived from observations of edge-on galaxies reveal that bulge kinematics vary smoothly with distance from the galaxies' central planes. Consequently, some estimate can be made of a bulge's major-axis kinematics by extrapolating off-axis observations down to the plane of the galaxy. We can thus estimate values of $\overline{v}_{\rm max}$ and σ_0 for galaxy bulges. Such analysis has shown that rotational velocities are, on average, higher for bulges than for comparable elliptical galaxies (Davies & Illingworth 1983, Kormendy & Illingworth 1982). Figure 11.7 shows that in bulges $(v/\sigma)^*$ is close to unity, implying that these systems are flattened by rotation.

Confirmation that bulges can be adequately described as rotationally-flattened systems has come from more complete model fitting. After allowing for the gravitational influence of the disk component, Jarvis & Freeman (1985) have shown that a simple rotationally-flattened model can reproduce both the photometric properties of edge-on bulges and the kinematics derived from spectra at many locations away from their major axes.

Study of the kinematics of edge-on bulges using multiple observations away from their major axes has also revealed that systems with boxy isophotes (§4.2.2) rotate cylindrically: their mean streaming velocities do not decline with distance from their central planes (Kormendy & Illingworth 1982). Such bulges have been modeled as rotationally-flattened axisymmetric systems (Rowley 1988), but the properties of boxiness and cylindrical rotation can also be ascribed to a prolate bar-like structure (see §4.4.7).

11.3.2 Disk kinematics

As we have discussed above, we can only measure uncontaminated stellar disk kinematics by looking away from the central bulge region. Unfortunately,

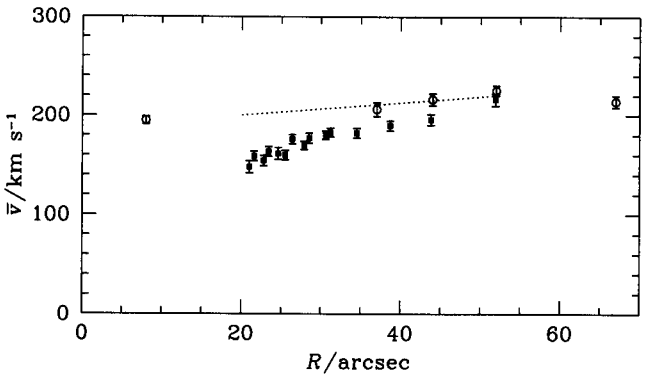

Figure 11.17 The mean rotation velocity for both gas (open circles) and stars (filled squares) in the disk galaxy NGC 488. The gaseous rotation curve is adapted from Peterson (1980a), and the stellar data are taken from Gerssen, Kuijken & Merrifield (1997). The dotted line shows the circular speed for this galaxy predicted purely from the stellar kinematics.

since the luminosity of a disk drops exponentially with radius (§4.4), these outer parts of disks are quite faint. We must therefore either make very long observations to obtain the requisite signal in the outer parts of galaxies, or try to decompose the complex kinematics at smaller radii into the separate disk and bulge contributions.

Rotational motion Kinematic studies of the disks of external galaxies reveal that, in all but face-on systems, $\overline{v}_{\rm los} \gg \sigma_{\rm los}$ at all radii: the stars in other disk galaxies, like those in the disk of the Milky Way (§10.3), follow approximately circular orbits with little random motion. We can therefore apply methods developed for calculating rotation curves from gas disks (§8.2.4) to the values of $\overline{v}_{\rm los}$ obtained from stellar spectra. Generally, the rotation curves derived from stellar observations have similar properties to those obtained from gas: the stellar rotation increases rapidly with radius near the center of the galaxy, and then flattens out to an approximately constant value. The similarity between the rotation curves from these two different populations confirms that the disk stars follow orbits similar to the circular motions of the gaseous component. Note, though, that the outer parts of disk galaxies are optically very faint, so it is not possible to measure stellar kinematics to the large radii that the HI data allow. Stellar rotation curves do not, therefore, provide any evidence for dark halos.

Figure 11.17 shows the rotation curves of both the gaseous and stellar components of the disk of the Sb galaxy NGC 488. The stellar kinematics are limited in extent by the faintness of the disk at large radii, and contam-

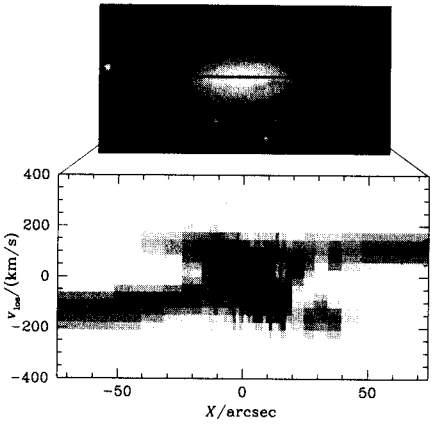

Figure 11.18 Stellar PV diagram for the major axis of the Sa galaxy NGC 3593 (as marked on the accompanying image). The kinematics were derived using the UGD algorithm. [DSS image from the Palomar/National Geographic Society Sky Survey, reproduced by permission; the kinematic data were obtained by M. Merrifield and K. Kuijken]

ination by the bulge component for $R < 20$ arcsec. The gaseous kinematics contain a gap at radii around 20 arcsec since there are no measured emission lines in this region. Where the data do overlap, it is clear that there is a small systematic offset between the two rotation curves. This offset is the asymmetric drift that we have already encountered in the solar neighborhood (§10.3.1). It arises because stars do not follow purely circular orbits, but have some random component to their motions (BT §4.2). As in the Milky Way, the measured asymmetric drift can be used to characterize the size of this random motion relative to the ordered streaming (see below).

As we have seen in §8.2.5, comparisons between the gaseous and stellar rotation curves of S0 galaxies have turned up the unexpected result that, in a significant minority of cases, these species rotate in opposite directions. These small counter-rotating gas disks in S0 galaxies could well arise from the late accretion and tidal disruption of small satellite galaxies. Rather harder to explain is the case of NGC 3626, in which as much as $10^9\,\mathcal{M}_\odot$ of hydrogen (atomic and ionized) counter-rotates relative to the stars across a wide radial range (Ciri, Bettoni & Galletta 1995).

The strangest counter-rotating disk phenomenon of them all, however, is exemplified by NGC 4550. Absorption features in spectra of this apparently-normal edge-on S0 galaxy were found to have a double structure (Rubin, Graham & Kenney 1992), and analysis of the galaxy's LOSVDs showed that these features arise because 50% of the stars in the disk of this galaxy follow approximately circular orbits in one direction, while the other 50% follow similar orbits in the opposite direction (Rix *et al.* 1992).[4] A handful of similar systems have now been identified. For example, Bertola *et al.* (1996) found clear signs of a small counter-rotating stellar disk in the kinematics of

[4] Such a bimodal velocity distribution provides an example of a case where the kinematics cannot be derived using a method which assumes that the LOSVD is anywhere near Gaussian in shape.

the Sa galaxy NGC 3593. As Figure 11.18 illustrates, this counter-rotation shows up clearly in the galaxy's stellar PV diagram. Since there are relatively few galaxies for which spectra have been obtained of the quality necessary to produce PV diagrams, the fraction of galaxies that contain counter-rotating disks remains uncertain. However, a study by Kuijken, Fisher & Merrifield (1996) indicates that less than $\sim 10\%$ of S0 galaxies contain even modest counter-rotating components, so these objects are probably quite rare.

Random motions As discussed above, we can infer the presence of non-circular stellar motions by observing asymmetric drift. In principle, we can obtain a direct measure of the random component of the stellar motions by extracting values of $\sigma_{\rm los}$ from spectra. If we define the usual cylindrical polar coordinate system, (R, ϕ, z), aligned with the axis of symmetry of the disk, then spectra of face-on galaxies provide a measure of the z-component of the stars' velocity dispersion, σ_z, whereas observations of edge-on systems allow us to measure a combination of the R- and ϕ-components, σ_R and σ_ϕ. Of course, all that we can observe directly is the average velocity dispersion integrated along the line of sight. Further, the usual techniques for measuring kinematics do not allow for the differences that we would expect to find in stars of different ages (c.f. the Milky Way, §10.3.2), but rather they produce some weighted average kinematics depending on the choice of template star. Some care must therefore be taken when converting the observed kinematics into localized measurements of the dynamics of disks.

In practice, even line-of-sight averaged quantities are difficult to observe. Face-on disks are intrinsically very faint, and the random motions in the z-direction tend to be small. It is therefore difficult to obtain spectra at sufficiently high signal-to-noise ratios for σ_z to be measurable. For edge-on systems, we have seen that the broadening of the LOSVD is dominated by the different projections of the rotational velocity that one sees along any given line of sight. In order to measure the relatively small contribution to the total broadening of the LOSVDs due to the random stellar motions in the R- and ϕ-directions, we must be able to characterize accurately the total width and shape of the velocity distributions. Once again, data obtained using high throughput spectrographs on large telescopes are beginning to overcome these difficulties. Observations of a dozen or so galaxy disks with a range of orientations have allowed us to characterize the variations in the components of velocity dispersion with radius – for a summary, see Bottema (1993).

Observations of face-on galaxies show that σ_z declines exponentially with radius. This relation has a simple physical interpretation: from the equations of stellar dynamics, it is straightforward to show that, for a thin disk,

$$\sigma_z^2 = 2\pi G \Sigma z_0, \tag{11.15}$$

where Σ is the surface density of the disk, and z_0 is a characteristic measure of the scale-height of the disk perpendicular to the plane (see Problem 11.7).

If z_0 does not vary with radius (as observations of edge-on galaxies suggest; §4.4), then $\sigma_z \propto \sqrt{\Sigma}$. We also know that the surface brightness of galaxies follows the exponential law, $I = I_0 \exp(-R/R_\mathrm{d})$ (§4.4). Therefore, if mass follows light so that $\Sigma \propto I$, we would expect σ_z to decline exponentially with radius with an e-folding length of $2R_\mathrm{d}$. Comparisons between kinematic and photometric measurements reveal that σ_z does, indeed, decline with a scale-length of approximately twice that of the surface brightness (Bottema 1993). Note, however, that the photometric scale-lengths used in this analysis were generally based on optical measurements, and, as mentioned in §4.4, the infrared scale-lengths of disks tend to be systematically smaller. Since the infrared photometry is more likely to reflect the underlying mass distribution, the above simple analysis is not secure.

Evaluation of the other two components of the velocity dispersion is more complicated since both contribute to σ_los in observations of inclined galaxies, and there is the additional contribution to the broadening of the LOSVD from the projection of the mean streaming. Modeling of the observed values of σ_los from edge-on galaxies has revealed that, like σ_z, σ_R and σ_ϕ decline approximately exponentially with radius with an e-folding length twice that of the disk surface brightness (Bottema 1993). We might therefore tentatively conclude that the ratio between the different components of random stellar motions remains approximately constant, and hence that the shape of the velocity ellipsoid (see Box 10.2) in disk galaxies does not vary dramatically with radius.

Note that the inference that we have drawn as to the constant shape of the velocity ellipsoid is rather indirect. We have measured the z-component of the random motions from observations of face-on galaxies, and the other two components from observations of other systems with edge-on orientations. In fact, it is possible to estimate all three components in a single a disk-dominated galaxy that has intermediate inclination i. When we observe such a galaxy at some point R from its center along its major axis the observed dispersion is given by

$$\sigma^2_\mathrm{maj}(R) = \sigma^2_\phi \sin^2 i + \sigma^2_z \cos^2 i. \tag{11.16}$$

The annulus of radius R within the disk cuts the apparent minor axis at a distance $R\cos i$ from the center. Here we will find a line-of-sight velocity dispersion

$$\sigma^2_\mathrm{min}(R\cos i) = \sigma^2_R \sin^2 i + \sigma^2_z \cos^2 i. \tag{11.17}$$

Thus, by measuring the variations in the line-of-sight dispersions along the principal axes, we can measure two linear combinations of $\sigma_R(R)$, $\sigma_\phi(R)$ and $\sigma_z(R)$. To close this system of equations, we can turn to the theory of stellar dynamics, which shows how dispersion components are related to one another. For example, if the epicycle approximation (BT §4.2) is valid, then

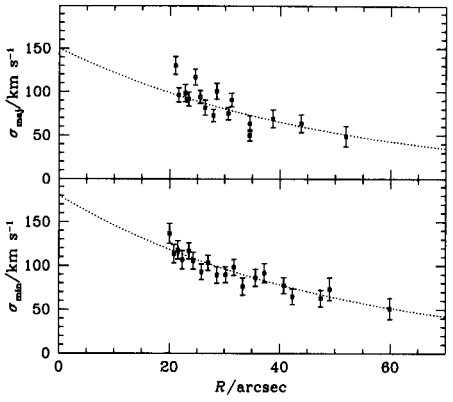

Figure 11.19 The line-of-sight stellar velocity dispersion observed along the major and minor axes of NGC 488. The dotted lines shows a simple stellar kinematic model fitted to these data. [After Gerssen, Kuijken & Merrifield (1997)]

the radial and tangential dispersions are simply related to the circular speed, v_c:

$$\frac{\sigma^2_\phi}{\sigma^2_R} = \frac{1}{2}\left(1 + \frac{\mathrm{d}v_c}{\mathrm{d}R}\right) \tag{11.18}$$

[equation (4-52) of BT, with the Oort constants replaced by the definitions of §10.3.3]. The circular speed itself can be obtained from the rotational velocities of the stars, corrected for asymmetric drift [see above and BT equation (4-34)]. It is thus possible to solve for $\sigma_R(R)$, $\sigma_\phi(R)$, $\sigma_z(R)$ *and* $v_c(R)$ just from the observed mean velocity along the major axis, $\overline{v}_\mathrm{maj}(R)$, combined with the line-of-sight dispersions, $\sigma_\mathrm{min}(R)$ and $\sigma_\mathrm{maj}(R)$.

The first application of this technique has been made by Gerssen, Kuijken & Merrifield (1997). Figure 11.19 shows the results of fitting a simple model that meets the above requirements to the observed major- and minor-axis dispersions of NGC 488 [as well as $\overline{v}_\mathrm{maj}(R)$ – see Figure 11.17]. A check on this model fit is provided by the predictions made for the circular speed, $v_c(R)$, which can be compared to the observed gaseous rotation velocities – see Figure 11.17. The results of this analysis indicate that the components of the stellar velocity ellipsoid in NGC 488 are in the approximate ratio $\sigma_R{:}\sigma_\phi{:}\sigma_z \approx 1{:}0.8{:}0.7$. Thus, the ordering of these components is the same as for the giant stars in the solar neighborhood of the Milky Way (Table 10.3), the only other place in which this ratio has been measured. More detailed comparisons between the velocity ellipsoids of disk galaxies must await observations of larger samples of these systems, and more sophisticated modeling of higher-quality data.